ISIJ International, Vol. 54 (2014), No. 1, pp. 212–221

Tensile Behavior of Ti,Mo-added Low Carbon Steels with Interphase Precipitation

Naoya KAMIKAWA,[1)]* Yoshihisa ABE,[2)] Goro MIYAMOTO,[1)] Yoshimasa FUNAKAWA[3)] and Tadashi FURUHARA[1)]

1) Institute for Materials Research, Tohoku University, 2-1-1 Katahira, Aoba-ku, Sendai, 980-8577 Japan.
2) Formerly Graduate Student, Tohoku University. Now at JFE Steel Corporation, 1 Kokan-cho, Fukuyama, 721-8510 Japan.
3) Research Planning & Administration Department, Steel Research Laboratory, JFE Steel Corporation, 1 Kawasaki-cho, Chuo-ku, Chiba, 260-0835 Japan.

(*Received on June 13, 2013; accepted on August 19, 2013; originally published in Tetsu-to-Hagané, Vol. 98, 2012, No. 6, pp. 245–252*)

Tensile behavior and structure-property relationship of ferritic steels with nano-sized carbide dispersion were invesigated using Ti-added steel and Ti,Mo-added low carbon steels. By austenitizing followed by isothermal heat treatment at 700°C, polygonal ferrites containing very fine carbides of TiC and (Ti,Mo)C were obtained in the Ti-added and the Ti,Mo-added steels, respectively. The size of such carbides was finer in the Ti,Mo-added steel than in the Ti-added steel at the same isothermal holding. The results of tensile tests for these samples showed that the strength is higher as the carbide size is smaller. The structure-based strength calculation led to a good agreement with the experiments, when it was assumed that the Ashby-Orowan mechanism is dominant for precipitation strengthening of nano-sized alloy carbides. It was also suggested that a relatively large tensile ductility is related to enhanced recovery during the tensile deformation, accompanied with promotion of secondary slips or cross slips in a finer scale due to the nano-sized particles.

KEY WORDS: low carbon steel; interphase precipitation; precipitation strengthening; work hardening; ductility.

1. Introduction

Dispersion of fine carbides is one of the methods to improve strength of structural steels.[1–3)] Cementite particles have widely been used as one of such obstacles for strengthening. However, diffusion of carbon atoms in iron is quite fast, leading to easy coarsening of the particles, which could degrade the strength of materials. On the other hand, in alloyed steels containing strong carbide forming elements, such as Ti, V, Mo, Nb, since alloying elements cannot diffuse as fast as carbon atoms, very fine carbides with an average diameter of a few nanometers to several tens nanometers can be obtained by controlled thermo-mechanical treatments.[3–5)]

Precipitation of alloy carbides can occur in different manners, which can be classified into three main categories: (i) precipitation in supersaturated austenite, (ii) precipitation on austenite/ferrite interface and (iii) precipitation in supersaturated ferrite. Among these categories, the second category is termed interphase precipitation, or interphase boundary precipitation, where alloy carbides repeatedly nucleates on austenite/ferrite interfaces during ferrite transformation from austenite, which often leads to a periodic dispersion of nano-sized carbides in row.[6–12)] Interphase precipitation is effective to obtain a relatively uniform distribution of nano-sized carbides since nucleation of alloy carbides always takes place on the interfaces. Moreover, by interphase precipitation, nano-sized carbide structures can be formed within ferrite during cooling process from high-temperature austenite, without any re-heating process that is normally required *e.g.* for tempering of quenched martensite. Therefore, more attention has recently been paid to interphase precipitation as a process to produce high tensile strength low alloy steels at low cost. It has been reported that ferritic steels with nano-sized alloy carbides produced by interphase precipitation show both very high strength and good formability, and some kinds of alloy steels have already been in commercial use.[13–16)]

Many studies have been reported on mechanical properties of interphase precipitated steels so far,[17–23)] but effects of nano-sized alloy carbides by interphase precipitation on strength and ductility of materials are not yet clear. In the present study, ferrite single phase steels with nano-sized alloy carbides were prepared using Ti,Mo-added low carbon steels, and tensile behavior of the samples were systematically investigated. The effect of nano-sized carbides on yielding behavior, work hardening and ductility is discussed in detail.

2. Experimental

Two kinds of low carbon steels with a basic composition of 0.04%C, 0.02%Si and 1.3%Mn in mass% were used in this study. One contains small amount of Ti, and the other contains both Ti and Mo, which are referred to as Ti-added and Ti,Mo-added steels, respectively. In Ti-added steel, the atomic ratio of C and Ti has been designed to be 1:1, while in Ti,Mo-added steel the atomic ratio of Ti and Mo is designed to be 1:1 and the sum of Ti atoms and Mo atoms is equal to C atoms. Ingots of both steels were prepared by vacuum melting and hot rolled to 20 mm in thickness at a

* Corresponding author: E-mail: kamikawa@imr.tohoku.ac.jp
DOI: http://dx.doi.org/10.2355/isijinternational.54.212

final rolling temperature of ~1 000°C, which has been used as starting materials. For both steels, starting samples were heat treated in vacuum at 1 250°C for 600 s for austenitization as well as solid solution treatment, and then isothermally transformed in a salt bath at 700°C for different holding periods in the range from 60 s to 172.8 ks (48 h) to lead to ferrite transformation accompanied with interphase precipitation of alloy carbides, followed by ice brine quenching.

Microstructures of the heat treated samples were characterized by optical microscopy, electron backscatter diffraction (EBSD) in a scanning electron microscope (SEM) and transmission electron microscopy (TEM). Longitudinal sections perpendicular to the transverse direction (TD) of the hot rolled sheets were prepared for the observations. For optical microscopy, the TD planes were mechanically polished by SiC paper and diamond paste, and etched by a solution of 3 vol.% HNO_3 (nitric acid) + 97 vol.% C_2H_5OH (ethanol). For EBSD measurements, polished surfaces were prepared in the same way as for the optical microscopy, and orientation mapping was carried out using a software TSL OIM Data Correction in an FEI Quanta 3D SEM operating at 25 kV. The obtained data was analyzed by a software TSL OIM Analysis. For TEM observations, thin foils of TD planes were prepared by mechanical polishing followed by twin-jet electro-polishing in a solution of 10 vol.% $HClO_4$ (HClO4) + 90 vol.% CH_3COOH (acetic acid) at 12°C at a voltage of 12–14 V.

Mechanical properties of the samples were determined by uniaxial tensile test at room temperature. Tensile specimens with a gauge length of 10 mm, width of 5 mm and thickness of 1 mm were prepared, where the tensile direction was parallel to the rolling direction of the hot rolled sheets. Tensile tests were carried out at a constant crosshead speed of 0.5 mm minute^{-1}, corresponding to an initial strain rate of 8.3×10^{-4} s^{-1}. Tensile elongation was measured by a clip-on extensometer.

To understand the work hardening behavior of the interphase precipitated samples, dislocation structures developed during tensile test were observed by TEM. Tensile tests were carried out under the same condition described above. The tensile tests were interrupted at different plastic tensile strains, unloaded and subject to TEM observations. For comparison, ultralow carbon interstitial free (IF) steel with a chemical composition of Fe-0.0023mass%C-0.01%Si-1.48%Mn-0.042%Ti was also used to emphasize the effect of nano-sized alloy carbides. Hot-rolled IF sheets were austenitized at 1 250°C for 600 s, and isothermally transformed in a salt bath at 700°C for 0.75 h (45 min) to obtain a fully transformed ferrite with an average grain size of 54 μm. Using this fully transformed IF steel, the evolution of dislocation structures during tensile tests were observed and compared with the results of interphase precipitated samples. Dislocation density (ρ_{dis}) for the as-transformed and tensile tested samples were measured from TEM images by Ham's method,[24] where the thickness of TEM foils was determined by convergent beam electron diffraction (CBED) technique.

3. Results

3.1. Optical Microstructures

Figure 1 shows optical microstructures of samples isothermally transformed at 700°C for different holding periods. For both steels, allotriomorphic or relatively equiaxed ferrite grains are observed mainly on austenite grain boundaries in the holding period of 20 s. The fraction of ferrite increases with increasing the holding period, and 1.8 ks (0.5 h) holding almost completes the transformation for both steels. The ferrite grain size was determined from EBSD measurements to 69 μm and 58 μm in the Ti-added and Ti,Mo-added steels, respectively. The isothermal transformation was carried out until 48 h holding, but the ferrite grain size was in the range of 60–70 μm for all cases. In other words, no significant grain growth of ferrite occurred during the prolonged holding.

3.2. Transmission Electron Microscopy (TEM)

Precipitation structures within the ferrite grains in the samples transformed at 700°C were observed by TEM. **Figures 2**(a) and 2(b) are TEM structures of the Ti-added and Ti,Mo-added samples transformed for 0.5 h, respectively, in which ferrite transformation has almost been completed for both steels. It is clearly seen that periodic sheets of nano-sized particles in row are formed within ferrite grains, typical for interphase precipitation. These precipitates are NaCl-type FCC structured alloy carbides. In the Ti-added steel the carbides are TiC with an atomic ratio of Ti and C of approximately 1:1, while in the Ti,Mo-added steel the carbides are (Ti,Mo)C,[17,18,25,26] where some of Ti atoms in TiC carbides are replaced by Mo atoms. The spacing of such particle sheets was approximately 25 nm and 20 nm in the Ti-added and Ti,Mo-added steels, respectively, *i.e.* there is no significant difference in the sheet spacing between two steels.

It is well known that NaCl-type alloy carbide (MC) precipitates in the ferrite (α) matrix with the following orientation relationship, so-called Baker-Nutting relationship.[27]

$$(100)_{MC} // (100)_{\alpha}$$
$$[010]_{MC} // [011]_{\alpha} \quad \text{..... (1)}$$

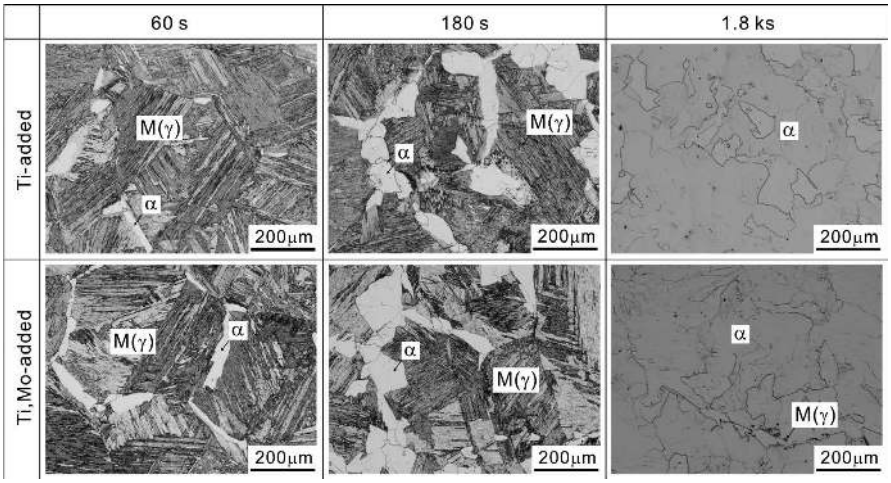

Fig. 1. Optical microstructures of the Ti-added and Ti,Mo-added steels isothermally transformed at 700°C for different holding periods.

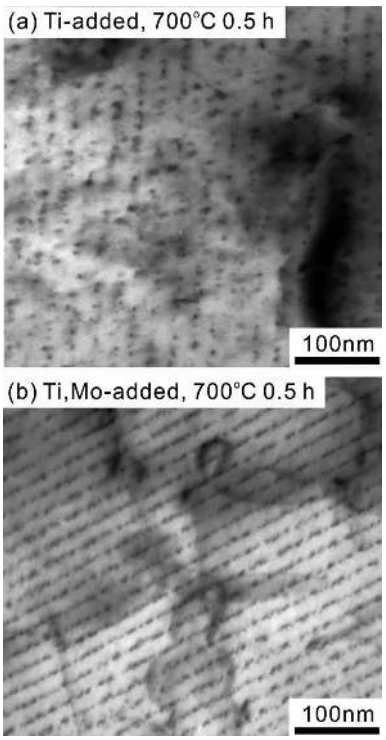

Fig. 2. TEM images showing the interphase precipitation in the Ti-added and Ti,Mo-added steels isothermally transformed at 700°C for 0.5 h.

In this relationship, {100} planes of MC and {100} planes of ferrite are coherent, so that MC carbides grow along habit planes of {100} ferrite, leading to a disc-shaped morphology of precipitates.[4,5] Alloy carbides can precipitate along three different {100} ferrite planes in the Baker-Nutting orientation relationship. In other words, there are three possible variants of MC in the ferrite matrix. However, in the case of interphase precipitation, only one variant of MC, whose habit place is most parallel to the austenite/ferrite interface, preferentially forms.[6,7,12] This is because that such variant selection can consume larger austenite/ferrite interfaces than other two variants when disc-shaped carbides nucleated, and the selected variant of carbides can grow very fast by interfacial diffusion along austenite/ferrite interfaces.[6,7,12] One may argue that such variant selection of MC in the interphase precipitation is related to the orientation relationship between the austenite and ferrite during the transformation, as reported by Honeycombe.[12] However, recent observations[28] have confirmed that in most cases ferrite grains accompanied with interphase precipitation grow with no specific orientation with respect to the adjacent austenite. It can therefore be considered that the variant selection of MC in the interphase precipitation is mainly due to the relationship between the orientation of austenite/ferrite interface and the habit plane of MC.

For the samples obtained in this study, variant selection of alloy carbides has been investigated using dark field imaging of carbides in TEM. **Figure 3** shows a schematic diagram of diffraction patterns with the electron beam direction parallel to [001] of ferrite, where ferrite and MC carbides have the Baker-Nutting orientation relationship. When the electron beam is chosen to be almost parallel to $[001]_{\alpha}$, two variants of carbides among three can be excited so that each variant can be imaged in dark-field. **Figure 4** are the TEM images with the incident beam almost parallel to [001] of ferrite in the Ti-added sample transformed at 700°C for 0.5 h. Two bright field images were taken from the exactly same area under different diffraction conditions of $g^*_{\alpha\text{-Fe}}$= 200 and $g^*_{\alpha\text{-Fe}}$=020. Dark field images were taken under

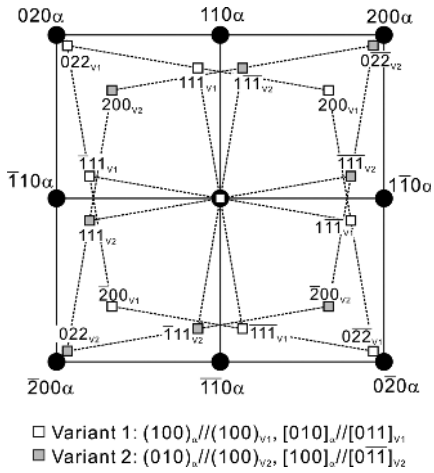

Fig. 3. Diffraction pattern of ferrite matrix and precipitated MC, where the matrix and MC has a Baker-Nutting orientation relationship. The incident beam is parallel to [001] of ferrite matrix. Two variants of MC (V1 and V2) are indicated.

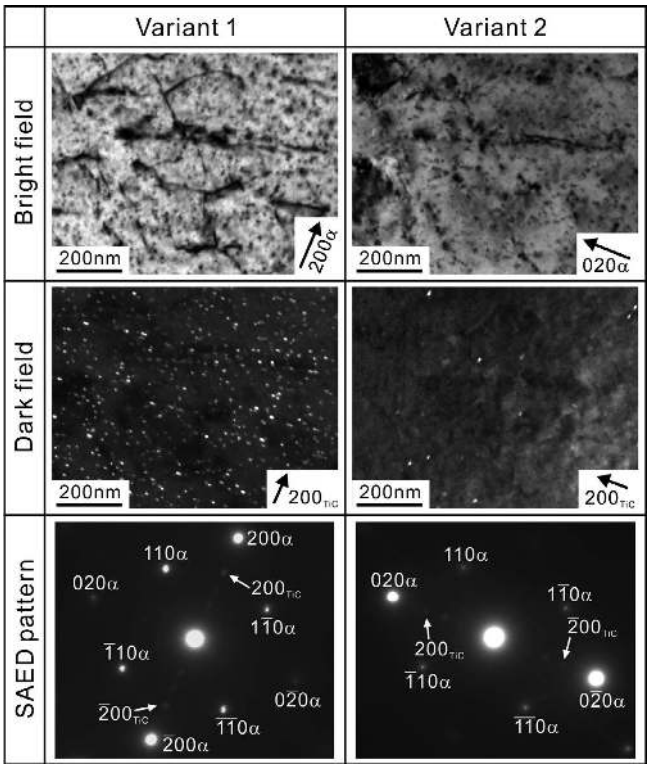

Fig. 4. TEM microstructures of the Ti-added steel isothermally transformed at 700°C for 0.5 h. The bright field images were taken under a condition of $g^*_{\alpha\text{-Fe}}$=200 or 020 and the dark field images under a condition of g^*_{TiC}=200. The corresponding selected area electron diffraction (SAED) patterns are indicated.

diffraction conditions of $g^*_{TiC\text{-}V1}$=200 and $g^*_{TiC\text{-}V2}$=200. Therefore, the following orientation relationship has been satisfied: $(100)_{\alpha\text{-Fe}}//(100)_{TiC\text{-}V1}$, $(010)_{\alpha\text{-Fe}}//(100)_{TiC\text{-}V2}$. It is clearly seen from the dark field images that a lot of carbides of variant 1 are observed while few carbides of variant 2 are observed. A similar variant analysis has been carried out for other two different areas, and the same trend that only one variant of carbides is dominated among three possibilities has been found for all cases. This suggests that single variant of carbides in the Baker-Nutting orientation relationship tends to nucleate dominantly when interphase precipitation occurs, in good agreement with the previous work.[6,7,12] For

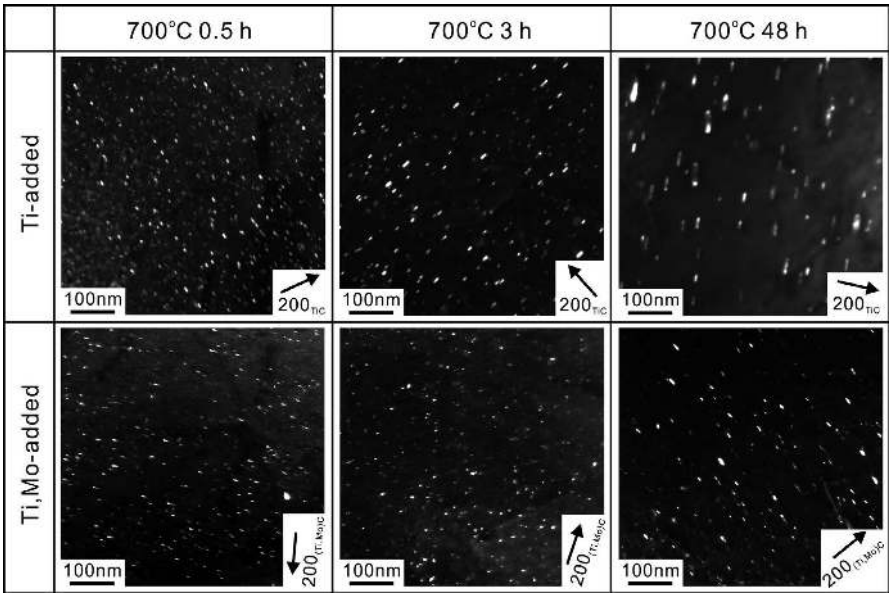

Fig. 5. Dark field TEM images for the samples isothermally transformed at 700°C for different periods. The images were taken under a condition of g^*_{MC}=200.

Ti,Mo-added steels, a similar tendency of single variant selection of carbides has been confirmed.

To see the change in the size of alloy carbides with increasing the holding period, dark field imaging in TEM has been done for precipitation structures of samples transformed for various holding periods in **Fig. 5**. The incident beam was parallel to [001] of ferrite matrix, and dark field images were obtained under a diffraction condition of g^*_{MC}=200. For all cases, disc-shaped precipitates are observed, and the disc planes are almost parallel to (100) plane of ferrite. This result is due to the fact that alloy carbides has grown along the (100) plane of ferrite with a habit plane of (100) of MC.

To determine the carbide size obtained from the TEM images, it is assumed that a MC carbide have a shape of oblate spheroid in three dimension, and that the diameter and thickness of the disc-shaped MC in the TEM images are the lengths in the minor and major axes of the oblate spheroid, respectively. Based on this assumption, the volume of the oblate spheroid was calculated, and a diameter of carbide was defined as a diameter of sphere that has the same volume of the oblate spheroid. Particle diameter distributions in the Ti-added and Ti,Mo-added samples transformed for different holding periods are shown for in **Fig. 6**. In the Ti-added sample transformed for 0.5 h (Fig. 6(a)), a relatively uniform distribution can be seen. The distribution is in the range from 2.3 nm to 12 nm, and the average diameter is 5.5 nm. Carbide size distributions in Ti-added low-carbon steels with interphase precipitated structures have quantitatively been investigated previously by three-dimensional atom probe tomography[29] or small-angle neutron scattering method,[30] and a minimum diameter of approximately 2 nm has been reported in both cases. Such results are in good agreement with the present result, indicating that the size distribution data obtained by TEM dark field imaging in this study is quantitatively reliable enough. On the other hand, in the Ti,Mo-added sample transformed for 0.5 h, the diameter distribution is in the range from 1.7 nm to 10 nm and the average diameter is 3.9 nm, which are smaller than those in the Ti-added steel transformed for 0.5 h. In the Ti-added steel, the carbide diameter increases with increasing the holding period, and after 48 h holding the average diameter is coarsened to 18 nm. The size distribution is still relatively uniform even after a prolonged holding. On the other hand, in the Ti,Mo-added steel, the carbide size increases with

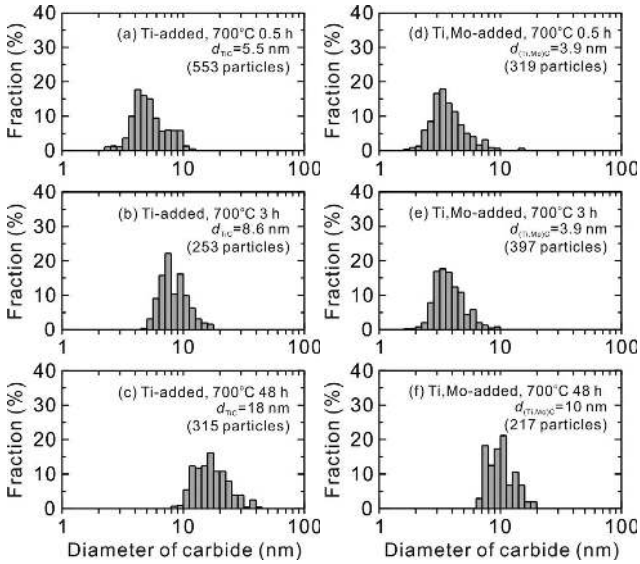

Fig. 6. Distributions of carbide diameter in the Ti-added and Ti,Mo-added steels transformed at 700°C for different holding periods. The diameters were determined by TEM dark-field images.

increasing the holding time, as for the Ti-added steel, but it changes more gradually. The average carbide size after 48 h holding is about 10 nm, smaller than that in the Ti-added steel (18 nm) for the same holding period. These results demonstrate that a simultaneous addition of Ti and Mo suppress the coarsening of alloy carbides, corresponding well with the fact reported by Funakawa *et al.*[18]

Funakawa *et al.*[18] has reported that in a Ti,Mo-added steel the atomic ratio of Ti and Mo in (Ti,Mo)C particles is approximately 1:1 in the beginning of interphase precipitation, but the concentration of Ti became larger during coarsening of (Ti,Mo)C precipitates. In this situation, coarsening of precipitates would be controlled mainly by diffusion of Ti atoms. Since the solubility of Ti in the ferrite matrix is lower in the Ti,Mo-added steel than in the Ti-added steel, the coarsening of (Ti,Mo)C may be suppressed. To verify this hypothesis, chemical analysis of (Ti,Mo)C particles were carried out by electrolytic extraction and induction coupled plasma analysis for the present samples, and it has

been found that the atomic ratio of Ti and Mo in the (Ti,Mo)C particles is about 7:3, corresponding with the results of Funakawa *et al.*[18] Note also that thermodynamic calculation using Thermo-Calc has confirmed that solubility of Ti atoms in ferrite matrix is 23 mass ppm in the Ti-added steel and 0.52 mass ppm in the Ti,Mo-added steel, which leads to a slow coarsening of (Ti,Mo)C precipitates in the Ti,Mo-added steel. This discussion could explain the reason why the carbide size is smaller in the Ti,Mo-added steel than in the Ti-added steel in the present case as well.

3.3. Stress-strain Curves

Uniaxial tensile tests were carried out for the Ti-added and Ti,Mo-added samples with different particle sizes, and the results are shown in **Fig. 7**. From the stress-strain curves, 0.2% proof stress ($\sigma_{0.2}$), ultimate tensile strength (σ_{UTS}), uniform elongation ($e_{uniform}$) and total elongation (e_{total}) are determined and plotted as a function of holding periods in **Fig. 8**. The curve for the Ti-added sample transformed for 0.5 h, which has an average carbide diameter of 5.5 nm, shows yield stress of 420 MPa, ultimate tensile strength of 540 MPa, uniform elongation of 8% and total elongation of ~20%. The strength decreases and the elongation slightly increases with increasing the holding period, but the change in the elongation is not so significant (Fig. 8). A similar tendency can be seen in the Ti,Mo-added steel (Fig. 7(b)), but for the same holding period the strength of the Ti,Mo-added steel is larger than in the Ti-added steel. It should be emphasized that there is no big difference in the elongation between two steels (Fig. 8). These results indicate that the Ti,Mo-added steels show a better strength-ductility balance than the Ti-added steels. It should also be noted that for all cases the stress-strain curves can be characterized by high yield stress but relatively small work hardening, *i.e.* high yield ratio. This would be one of the characteristics for single phase ferrite steels with nano-sized alloy carbides.[19]

To understand such stress-strain behaviors of interphase precipitates samples, a relationship between precipitation structures and mechanical properties will be discussed in detail in the next section.

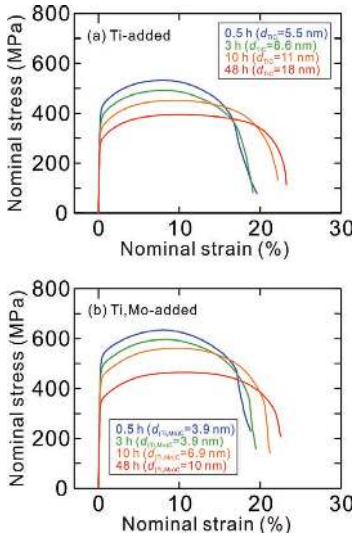

Fig. 7. Nominal stress-strain curves for the Ti-added and Ti,Mo-added steels isothermally transformed at 700°C for different holding periods.

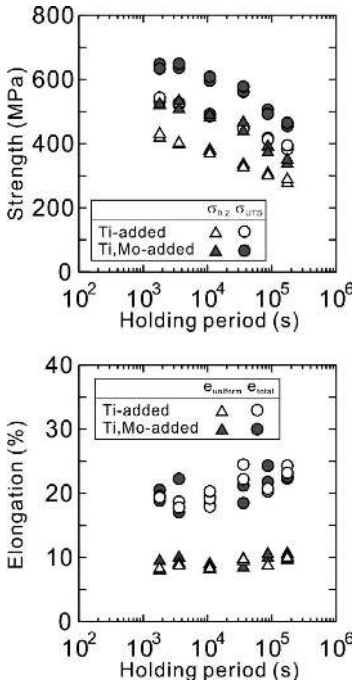

Fig. 8. Strength and elongation of the Ti-added and Ti,Mo-added steels isothermally transformed at 700°C for different holding periods.

4. Discussion

4.1. Strengthening Mechanisms of Nano-sized Alloy Carbides

As was shown in Figs. 7, 8, the samples with interphase precipitation in the present study have a higher yield stress as the carbide size is smaller, but detailed strengthening mechanisms of the samples are not clear yet. In this section, the strengthening mechanisms of nano-sized carbides is discussed quantitatively.

The strength of metals is determined by several different defects in the crystal, such as dislocations, solute atoms, precipitates and grain boundaries. It is assumed here that the yield stress of metals can be explained by a sum of strengthening contributions from each crystal defects in the following equation.

$$\sigma_{0.2} = \sigma_0 + \sigma_{ss} + \sigma_{dis} + \sigma_{ppt} + \sigma_{gb} \quad \text{(MPa)} \quad \text{..... (2)}$$

where σ_0 is the friction stress of single crystal pure iron, σ_{ss} is the solid solution strengthening, σ_{dis} is the dislocation strengthening, σ_{ppt} is the precipitation strengthening and σ_{gb} is the grain boundary strengthening. Based on this equation, the precipitation strengthening contribution is estimated by subtracting the other contributions from the experimentally obtained 0.2% proof stress.

The dislocation strengthening was estimated based on the Bailey-Hirsch relationship,[31]

$$\sigma_{dis} = M\alpha Gb\sqrt{\rho_{dis}} \quad \text{(MPa)} \quad \text{..... (3)}$$

where M is the Taylor factor, α is a constant (= 0.24 [32]), G is the shear modulus (=81.6 GPa),[33] b is the Burgers vector (= 0.248 nm), and ρ_{dis} is the dislocation density (m^{-2}). For the Taylor factor, the average value of random textured bcc metals M=2.75 was used where <111>-pensile glide has been assumed.[34] The dislocation density in the as-transformed state was measured by the TEM images. The term $\sigma_0+\sigma_{ss}+\sigma_{gb}$ was estimated using the Hall-Petch relationship[35,36] for the ultralow carbon IF steel (see Experimental). Since this IF steel contains a similar amount of Si and Mn to the Ti-added or Ti,Mo-added steels, it can be assumed that the solid solution strengthening and grain boundary strengthening is also similar to the Ti-added and Ti,Mo-added steels. The Hall-Petch relationship was experimentally obtained from IF samples with different grain sizes produced by cold rolling and recrystallization as follows.

$$\sigma_0 + \sigma_{ss} + \sigma_{gb} = \sigma_0' + kd_{gb}^{-1/2} = 74 + 210d_{gb}^{-1/2} \quad \text{(MPa)} \quad (4)$$

where d_{gb} (μm) is the ferrite grain size. Boundaries with misorientation angle above 2° were taken into account and intercept method with random test lines was used for the grain size determination. The strengthening contribution in Eq. (4) was calculated by using the ferrite grain size for each samples determined by the EBSD measurements. This term has been calculated to be approximately 100 MPa for all cases, which corresponds to the yield stress of fully recrystallized IF steels with no VC precipitation. Subtracting the contributions of Eqs. (3) and (4) from the experimentally determined 0.2% proof stress, the strengthening contribution from precipitates was estimated in the following.

$$\sigma_{ppt,\exp} = \sigma_{0.2,\exp} - \left(\sigma_0 + \sigma_{ss} + \sigma_{dis} + \sigma_{gb}\right) \quad \text{(MPa)} \quad (5)$$

Table 1 summarizes the structural parameters used and each strengthening contributions. It is seen from this table that dislocation strengthening has a relatively large contribution to the yield stress, but precipitation strengthening from nano-sized alloy carbides has a significant effect on strength of the interphase precipitated steels.

Figure 9 plots the obtained precipitation strengthening as a function of the average radius of alloy carbides. The precipitation strengthening is larger as the carbide radius is smaller, and it is seen that the maximum strengthening is as high as 300 MPa when the radius is about 2 nm. It is also seen that the plots of each data are on the same single curve, regardless of the alloys. These results indicate that Orowan-type mechanism[37–39] is dominant for the nano-sized alloy carbides obtained in the present study. Funakawa *et al.*[17] have reported that the precipitation strengthening can be estimated to be approximately 340 MPa for the (Ti,Mo)C alloy carbides with the average radius of 1.5 nm. Their data point is plotted in Fig. 9, in good agreement with the tendency in the present results. This also suggests that a similar strengthening mechanism is dominant for all cases.

To verify the above hypothesis, dislocation structures were observed after tensile deformation. **Figure 10**(a) shows the TEM image after 1% tensile strain for the Ti-added steel transformed for 0.5 h, having the carbide diameter of 5.5 nm. Even though only 1% of tensile strain has been applied, a number of dislocations are present in the sample. Some of the dislocations are pinned by the carbide particles and significantly bended, as arrows point out in the figure. This indicates that the nano-sized alloy carbides truly act as obstacles for dislocations. The Ti-added steel transformed for 48 h, with the average carbide diameter of 18 nm, was tensile tested to 10% strain, and dislocation structures were observed in Fig. 10(b), where a number of dislocation loops were clearly observed. Such dislocation loops should be created by interaction between moving dislocations and alloy carbides, since the size of dislocation loops is comparable with the diameter of the alloy carbides. This observation is a direct evidence to prove that the nano-sized alloy carbides obtained by interphase precipitation contribute the strength via an Orowan-type precipitation strengthening mechanism.

To understand whether the Orowan-type mechanism is valid for the nano-sized alloy carbides, the precipitation strengthening from the alloy carbides are estimated. In this estimation, two types of Orowan mechanisms are considered: the conventional Orowan mechanism and the Ashby-Orowan mechanism. In the conventional Orowan mechanism, the precipitation strengthening can be calculated as follows.[38,39]

$$\sigma_{\text{Orowan}} = \frac{0.8MGb}{L} \quad \text{(MPa)} \quad (6)$$

L is the average spacing between the precipitates, and can

Table 1. Structure-based strength calculation for Ti-added and Ti,Mo-added steels.

	d_{gb} μm	ρ_{dis} m^{-2}	$\sigma_{0.2,\exp}$ MPa	$\sigma_0+\sigma_{ss}+\sigma_{gb}$ MPa	σ_{dis} MPa	$\sigma_{ppt,\exp}$ MPa
Ti-added steel						
700°C 0.5 h	69	9.6×10^{13}	424	99.5	131	194
700°C 3 h	68	3.9×10^{13}	379	99.5	83.9	196
700°C 10 h	59	2.6×10^{13}	330	102	68.1	160
700°C 48 h	74	3.3×10^{13}	283	98.5	76.2	108
Ti,Mo-added steel						
700°C 0.5 h	58	6.6×10^{13}	522	102	108	311
700°C 3 h	51	3.8×10^{13}	485	103	81.8	300
700°C 10 h	52	5.3×10^{13}	452	103	97.1	252
700°C 48 h	57	5.3×10^{13}	344	102	97.3	144

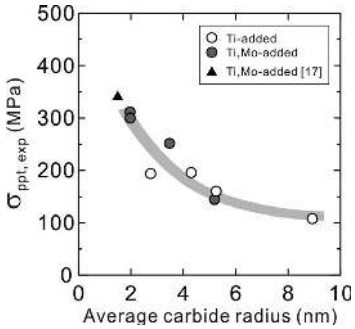

Fig. 9. Precipitation strengthening experimentally determined as a function of average carbide radius for the Ti-added and Ti,Mo-added steels transformed at 700°C for different holding periods. It has been assumed that strengthening contributions from solute atoms, dislocations, precipitates and grain boundaries are all additive, based on Eq. (2).

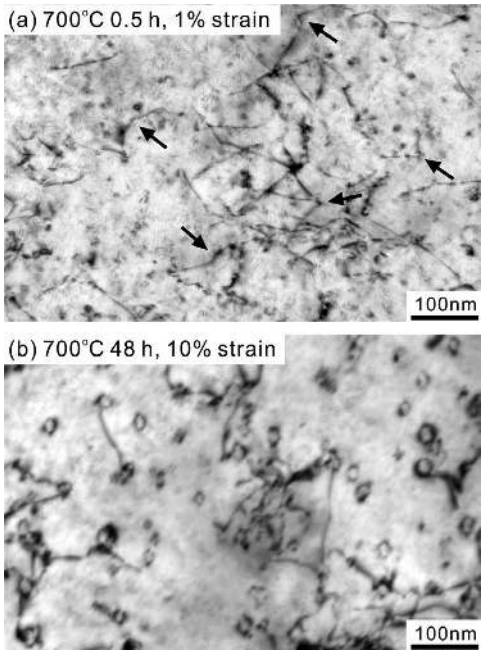

Fig. 10. TEM images of the Ti-added samples isothermally transformed and deformed in tension. (a) 700°C 0.5 h, 1% tensile tested, (b) 700°C 48 h, 10% tensile tested.

be calculated in the following, assuming that the precipitates are randomly distributed.[1)]

$$L = \sqrt{\frac{2}{3}}\left(\sqrt{\frac{\pi}{f}} - 2\right) \cdot r \quad \text{(m)} \qquad (7)$$

where r is the average radius and f is the volume fraction of alloy carbides. On the other hand, in the Ashby-Orowan mechanism, the conventional Orowan mechanism has been modified considering the interaction between two dislocation lines with opposite signs in the vicinity of a fine particle. The strengthening contribution by the Ashby-Orowan mechanism can be written as,[38,39)]

$$\sigma_{\text{Ashby-Orowan}} = \frac{0.8MGb}{2\pi\sqrt{1-\nu}L} \cdot \ln\left(\frac{x}{2b}\right) \quad \text{(MPa)} \qquad (8)$$

where ν is the Poisson's ratio (= 0.293 [33)]) and x is the average diameter of cross section of the alloy carbides on the slip planes.

$$x = 2\sqrt{\frac{2}{3}} \cdot r \quad \text{(m)} \qquad (9)$$

Based on these two Orowan-type mechanisms, the precipitation strengthening was calculated. For the calculation, the average radius of the alloy carbides was used from the TEM microstructures in Fig. 6, and the volume fraction of alloy carbides was obtained from the equilibrium value in the Thermo-Calc software. The equilibrium volume fraction of MC was determined to be 0.35% and 0.17% in the Ti-added and Ti,Mo-added steels, respectively. **Figures 11**(a) and 11(b) plot the precipitation strengthening by the coventional Orowan mechanism and by the Ashby-Orowan mechanism, respectively, as a function of experimentally determined precipitation strengthening using Eq. (5). In the Orowan mechanism (Fig. 11(a)), the calculated strengthening contribution by is much larger than the experiment, and the deviation is more enhanced in the higher strength region. On the other hand, Fig. 11(b) demonstrates that the Ashby-Orowan mechanism can reasonably explain the precipitation strengthening of the nano-sized alloy carbides obtained by interphase precipitation.

The above results suggest that the Ashby-Orowan mechanism is dominant for the precipitation strengthening in the carbide diameter of about 4 nm and above. However, the strengthening mechanism would be possible to change from the Orowan-type mechanism into the cutting mechanism[40)] when the carbide diameter becomes smaller.[41)] Therefore, the precipitation strengthening mechanism in the carbide diameter of 1–2 nm or below is still unclear, and further experiments and analysis are necessary to understand the operating mechanisms.

4.2. Work Hardening Behavior and Ductility

The present work demonstrates that the stress-strain curves for the samples with dispersion of nano-sized alloy carbides are characterized by very high yield stress, relatively small working hardening, sufficient uniform elongation and large post-uniform elongation. In particular, it is interesting that the samples with smaller-sized alloy carbides show a very high strength and sufficient total elongation. It is well known that ductility of metals are closely related to work hardening behavior after the yielding. In this section, the effect of nano-sized alloy carbides on the work hardening behavior and ductility of the interphase precipitated steels will be discussed in detail.

It is well known in uniaxial tensile deformation of metals that necking occurs when the following plastic instability criterion has been satisfied,[42)]

$$\sigma > \frac{d\sigma}{d\varepsilon} \qquad (10)$$

where σ and ε is the true stress and true strain, respectively, and $d\sigma/d\varepsilon$ is the work hardening rate. The nominal stress-nominal strain curves in Fig. 7 were transformed into true stress-true strain curves where uniform deformation under the volume constant condition is assumed. Work hardening rate curves were obtained by differentiating the true stress with respect to the true strain. To obtain a smooth work hardening rate curve, the true stress-true strain curve was first transformed into a polynomial approximate curve in the range from the yield stress point to the maximum stress point, and the approximate curve was differentiated with respect to the strain.

The obtained working hardening rate curves are plotted in **Fig. 12**, together with the true stress-strain curves. For comparison, work hardening rate of IF steel sample with the average ferrite grain size of 54 μm were also plotted in the figure. The upper and lower figures show the whole curves

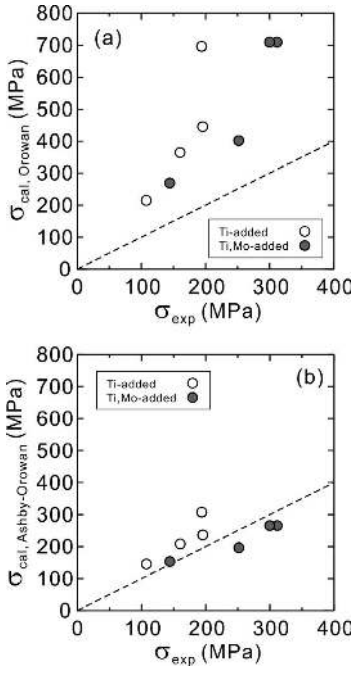

Fig. 11. Comparison between the experimentally determined precipitation strengthening and the calculated precipitation strengthening based on the Orowan mechanism (a) and the Ashby-Orowan mechanism (b).

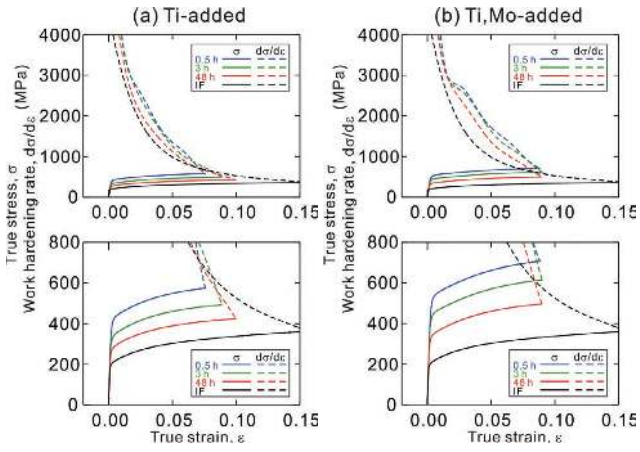

Fig. 12. True stress-true strain curves and work-hardening rate of the (a) Ti-added and (b) Ti,Mo-added steels isothermally transformed at 700°C for different holding periods. The result of the IF steel is also plotted for comparison.

and enlarged ones, respectively. It is seen that samples with alloy carbides show a larger work hardening rate than the IF steel with no carbides in the early stage of tensile deformation. In both Ti-added and Ti,Mo-added steels, there is no significant difference in work hardening curves in different holding periods, *i.e.* with different carbide sizes, but the work hardening rate tends to be larger as the carbide size is smaller. This result indicates that a decrease in the carbide size increases both strength and work hardening rate, leading to a retarded onset of plastic instability in tensile test. This could be the reason why the uniform elongation does not change even the carbide size is reduced. However, in the later stage of tensile test, the work hardening rate becomes lower in the samples containing alloy carbides than in the IF steel, indicating that dynamic recovery takes place significantly.

To understand the work hardening behavior observed, Ashby's work hardening theory is applied into the present experimental results. In Ashby's work hardening theory, it is suggested that work hardening can be explained by dislocation strengthening by geometrically necessary dislocations (GN dislocations) in the following equation,[43,44]

$$\sigma - \sigma_y = M\alpha Gb\sqrt{\rho_{GN}} \quad \text{..... (11)}$$

where σ_y is the yield stress, and ρ_{GN} is the density of GN dislocations. In the case of samples used in the present study, both nano-sized precipitates and grain boundaries can act as sites for generation of GN-dislocations. The density of GN dislocations produced in the vicinity of hard precipitates can be expressed as,[44]

$$\rho_{GN,ppt} = \frac{8f}{bd}\gamma \quad \text{..... (12)}$$

where d and f is the diameter and volume fraction of precipitates, respectively, and γ is the shear strain. By introducing the relationship of $\varepsilon = \gamma/M$, Eq. (12) can be rewritten as,

$$\rho_{GN,ppt} = \frac{8Mf}{bd}\varepsilon \quad \text{..... (13)}$$

On the other hand, the density of GN dislocations produced by grain boundaries is given by,

$$\rho_{GN,gb} = \frac{1}{4bd_{gb}}\varepsilon \quad \text{..... (14)}$$

Assuming that the total density of GN dislocations is a sum of $\rho_{GN,ppt}$ and $\rho_{GN,gb}$, the Eq. (11) can be described as,[45]

$$\begin{aligned}\sigma - \sigma_y &= M\alpha Gb\sqrt{\rho_{GN,ppt} + \rho_{GN,gb}} \\ &= M\alpha Gb\sqrt{\frac{8Mf}{bd}\varepsilon + \frac{1}{4bd_{gb}}\varepsilon} \quad \text{..... (15)} \\ &= M\alpha G\sqrt{b}\sqrt{\frac{8Mf}{d} + \frac{1}{4d_{gb}}}\sqrt{\varepsilon}\end{aligned}$$

Note in the present experiments that M of 2.75 is used, d is in the range of 4–20 nm, f is 0.35% or 0.17% in the Ti-added or Ti,Mo-added steels, respectively, and d_{gb} is 60–70 μm, so that the $\rho_{GN,ppt}$ would be much larger than $\rho_{GN,gb}$. Therefore, in this calculation, GN dislocations from grain boundaries are assumed to be negligible. Finally, work hardening can be assumed to be expressed by,

$$\sigma - \sigma_y = M\alpha G\sqrt{b}\sqrt{\frac{8Mf}{d}}\sqrt{\varepsilon} \quad \text{..... (15)}$$

Based on the above equation, work hardening curves are calculated and plotted in **Fig. 13**, where σ_y is taken as the proportional limit from the stress-strain curves. It is seen that the calculated stress-strain curves are in good agreement with the experimental curves only in the very beginning of tensile deformation, but they immediately starts to be positively deviated from the experiments. Such breakdown of Ashby's work hardening theory has also been reported, for instance, by Murakami *et al.*[46] in the work hardening behavior of ferrite steel containing VC particles with the average diameter of 40 nm,[46] where in the tensile strain up to 3% the work hardening behavior can be explained by the increase of dislocation density. It should be emphasized that in the present result the breakdown occurs in the very early stage of tensile test just after the yielding, suggesting that significant dynamic recovery of dislocations takes place already in the beginning of tensile deformation. In order to further understand the work hardening behavior of interphase precipitated steels, the change in dislocation structures has to be observed from the early stage and later stage of tensile deformation.

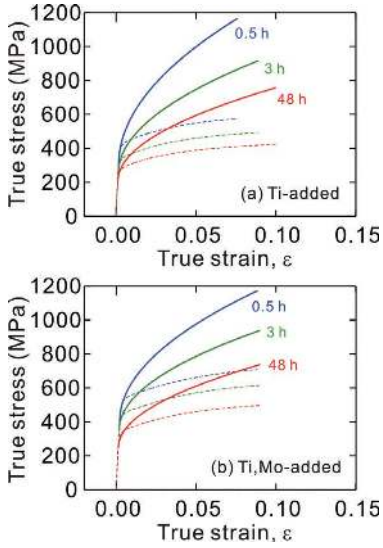

Fig. 13. Calculated stress-strain curves based on the Ashby's work hardening theory. Experimental curves are also plotted as dotted lines.

In this experiment, the Ti-added steels transformed for 0.5 h and 48 h and the Ti,Mo-added steel transformed for 0.5 h were tensile tested at room temperature up to different plastic strains, and the dislocation structures were observed by TEM. To emphasize the effect of alloy carbides, a similar experiment was carried out for the IF steel. **Figure 14** shows examples of the TEM structures for the Ti-added, 0.5 h transformed sample and IF steel. In the Ti-added sample transformed for 0.5 h having the average carbide diameter of 5.5 nm, a quite uniform dislocation structure is observed even after 1% of strain, and the dislocation density is already high. Yamada *et al.*[47] observed the dislocation structure after 0.2% plastic strain of the steel with nano-sized (Ti,Mo)C particles and found a high density of dislocations with a uniform distribution in the ferrite matrix, corresponding well with the resent observation. Tensile deformation of 5% strain leads to a higher density of dislocations in the Ti-added steel, but the dislocation distributions is quite uniform. Change in dislocation structures was also observed during the tensile test of the Ti,Mo-added steel transformed for 0.5 h, and a quite similar tendency has been observed. On the other hand, in the IF steel sample with no carbide, the dislocation density after 1% strain is quite low, and the dislocations are tangled and inhomogeneously distributed. Further deformation up to 5% increase the dislocation density and the dislocation cell structure starts to form in the IF steel sample, but the dislocation density is much lower than in the Ti-added sample.

Figure 15 is the change in the dislocation density with

increasing the plastic strain of tensile deformation. In the IF steel sample the dislocation density gradually increases with increasing the plastic strain, while in the interphase precipitated samples the density increases more rapidly than the IF steel. In particular, in the Ti-added and Ti,Mo-added samples with the average carbide size of 4–5 nm, this tendency is more significant. This observation indicates that nano-sized alloy carbides uniformly distributed in the ferrite matrix act as sites for dislocation multiplication. This could be due to that more complicated dislocation slips take place in the vicinity of hard TiC or (Ti,Mo)C particles, leading to enhanced work hardening by interactions of such multiplied dislocations in the early stage of tensile deformation. However, it is also seen that in the late stage of tensile deformation the dislocation density tends to be saturated for the samples with nano-sized carbides, indicating that dynamic recovery takes place significantly.

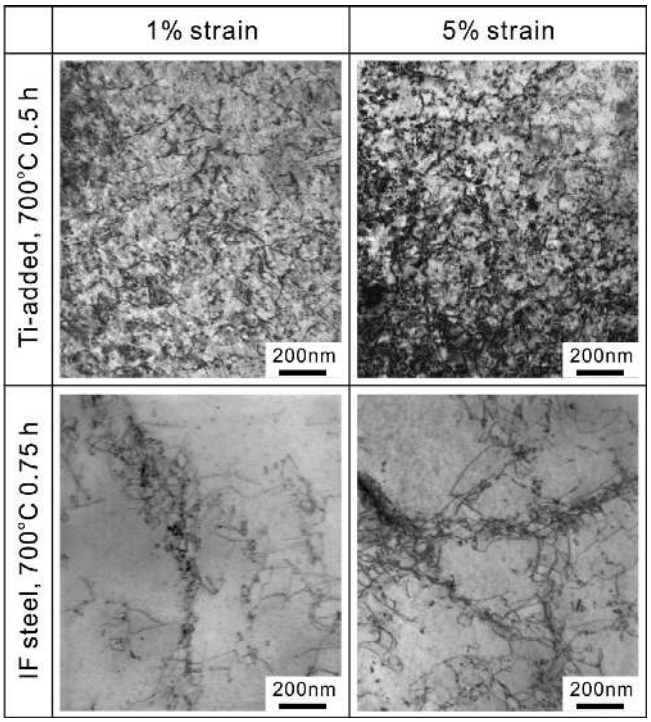

Fig. 14. Dislocation structures of the Ti-added and IF steel samples. Tensile tested to 1% and 5% in plastic strain.

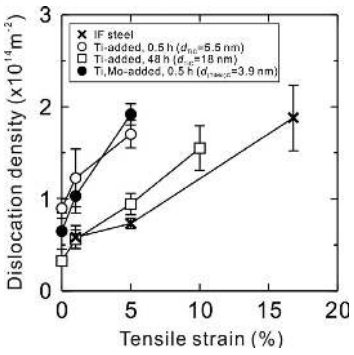

Fig. 15. Dislocation density as a function of tensile strain for the Ti-added and Ti,Mo-added steels isothermally transformed at 700°C for 0.5 h and 48 h. The data for IF steel is also plotted for comparison.

The change in the dislocation structures during tensile deformation of the interphase precipitated steels are schematically illustrated in **Fig. 16**. When the stress is applied for the samples with the uniform distribution of nano-sized alloy carbides, dislocations of primary slip system may start to operate first, and the yield stress significantly increases by the Orowan-type precipitation strengthening mechanism. In that case, moving dislocations pass though the particles, leaving dislocation loops around the particles. Due to the formation of such dislocation loops, the effective spacing of carbide particles becomes decreased. In addition, these dislocation loops may produce a large back stress against the following dislocations. For these reasons, the stress necessary for further dislocation movement would significantly increase.[40] For further deformation, additional dislocations of secondary slip system may be activated. Another mechanism is that cross slips of dislocation may occur very easily near the alloy carbides, since the carbide size is quite small. Secondary slip dislocations or cross slip dislocations may interact each other, leading to enhanced work hardening in the early stage of tensile deformation. However, in the later stage of deformation, such secondary slip or cross slip dislocations may easily be annihilated each other, *i.e.* dynamic recovery may occur significantly. This may retard the onset of plastic instability and improve the uniform elongation. The high yield ratio in the interphase precipitated steels can be understood by the enhanced dynamic recovery and supressed work hardening in the later stage of tensile deformation. If this enhanced dynamic recovery takes place in the necking deformation as well, dislocation pile-up would be suppressed and therefore formation of voids or cracks would also be delayed. This would be the reason why the interphase precipitated ferrite steels show relatively large post-uniform elongation.

This explanation could be applied to understand the effect of size or volume fraction of carbides on the mechanical properties. When the carbide size is smaller or the volume fraction is larger, the strength of the sample becomes larger. Moreover, since the density of carbide particles also becomes higher, sites for inhomogeneous deformation may also increase, leading to an enhanced work hardening in the early stage of deformation. In the later stage of deformation,

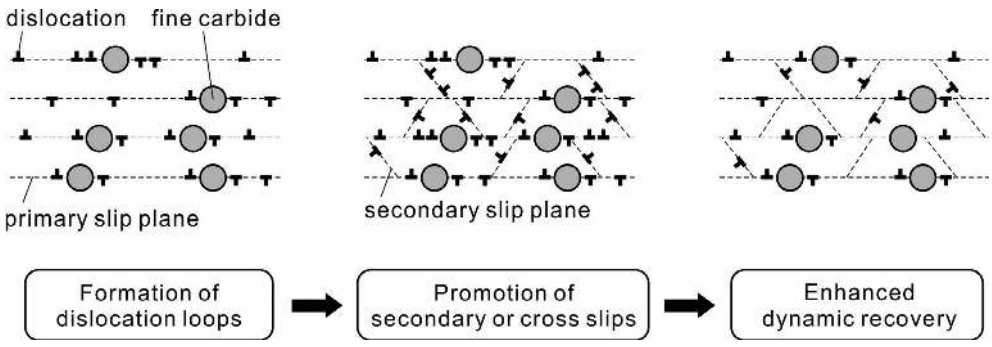

Fig. 16. Schematic illustration showing the change in dislocation structures during deformation of samples with a dispersion of fine carbides.

dynamic recovery may occurs more significantly if the carbide size is smaller or the volume fraction is larger, *i.e.* the density of carbides is higher, leading to an retarded formation of voids and cracks and improvement of post-uniform elongation.

In the present experiment, we have focused on the effect of carbide size on the strength, working hardening and ductility of the interphase precipitated samples. However, the effect of volume fraction on the mechanical properties is not yet clear. Therefore, further experiments to investigate the effect of volume fraction of carbides should be required to verify the above discussion. In addition, formation of voids or cracks should quantitatively be analysed in detail, and the fracture surface should also be observed to understand the mechanisms of ductile fracture of the interphase precipitated steels. These experiments will be a topic of forthcoming work.

5. Conclusions

In the present study, ferrite single phase samples with interphase precipitation of nano-sized alloy carbides were prepared using Ti-added and Ti,Mo-added low carbon steels, and the structure-property relationship was examined in detail. The results obtained can be summarized as follows.

(1) In both Ti-added and Ti,Mo-added steels, heat treatment at 700°C for 0.5 h led to ferrite transformation accompanied by interphase precipitation of alloy carbides with the average diameter of 4–5 nm. The coarsening of alloy carbides occurred by the prolonged holding, but smaller carbide size was observed in the Ti,Mo-added steel than in the Ti-added steel.

(2) The strength of the Ti,Mo-added steels was higher than that of the Ti-added steels for the same holding period, due to the smaller alloy carbide size in the Ti,Mo-added steel. However, the ductility of both steels were comparable, about 20% in total elongation. It is therefore suggested that dispersion of smaller-sized alloy carbides is more effective to obtain higher strength with sufficient ductility.

(3) Good agreement was observed between the experimentally determined yield stress and structure-based calculation, where additive law of strengthening contributions from solute atoms, dislocations, precipitates and grain boundaries was applied. It was suggested that strengthening contribution from nano-sized alloy carbides can be explained by the Ashby-Orowan mechanism.

(4) Uniformly dispersed nano-sized alloy carbides within ferrite matrix would play a significant role in increasing dislocation density in the beginning of deformation, leading to a large work-hardening. On the other hand, in the later stage of deformation, such dislocations multiplied in the vicinity of nano-sized carbides would significantly be annihilated each other, leading to enhanced dynamic recovery during deformation, which may improve both uniform and post-uniform elongation.

REFERENCES

1) A. Kelly and R. B. Nicholson: *Prog. Mater. Sci.*, **10** (1963), 149.
2) A. Kelly and R. B. Nicholson: Strengthening Methods in Crystals, Elsevier Publishing Company, Amsterdam, (1971).
3) H. K. D. H. Bhadeshia and R. W. K. Honeycombe: Steels, 3rd ed., Elsevier, Oxford, (2006).
4) E. Tekin and P. M. Kelly: *J. Iron Steel Inst.*, **203** (1965), 715.
5) D. Raynor, J. A. Whiteman and R. W. K. Honeycombe: *J. Iron Steel Inst.*, **204** (1966), 349.
6) A. T. Davenport, F. G. Berry and R. W. K. Honeycombe: *Metal Sci. J.*, **2** (1968), 104.
7) A. T. Davenport and R. W. K. Honeycombe: *Proc. Roy. Soc. Lond. A*, **322** (1971), 191.
8) A. T. Davenport and P. C. Becker: *Metall. Trans.*, **2** (1971), 2962.
9) D. V. Edmonds: *Metall. Trans.*, **4** (1973), 2527.
10) G. L. Dunlop and R. W. K. Honeycombe: *Philos. Mag.*, **32** (1975), 61.
11) S. Freeman and R. W. K. Honeycombe: *Metal Sci.*, **11** (1977), 59.
12) R. W. K. Honeycombe: Phase Transformation in Ferrous Alloys, ed. by A. R. Marder and J. Goldstein, Metall. Soc. AIME, Warrendale, (1983), 259.
13) K. Tomita, Y. Funakawa,T, Shiozaki, E. Maeda and T. Yamamoto: *Materia Jpn.*, **42** (2003), 70.
14) T. Shimizu, Y. Funakawa and S. Kaneko: *JFE Giho*, No. 4, (2004), 22.
15) N. Iwama, I. Nomura, M. Mori, M. Yano and T. Manabe: *Materia Jpn.*, **36** (1997), 622.
16) S. Niwa, I. Machida, T. Katoh, N. Uehara and Y. Tanaka: *Denki Seiko*, **53** (1982), 26.
17) Y. Funakawa, T. Shiozaki, K. Tomita, T. Yamamoto and E. Maeda: *ISIJ Int.*, **44** (2004), 1945.
18) Y. Funakawa and K. Seto: *Tetsu-to-Hagané*, **93** (2007), 49.
19) N. Kamikawa, Y. Abe, G. Miyamoto and T. Furuhara: Proc. 2nd Int. Symp. Steel Sci. (ISSS 2009), ISIJ, Tokyo, (2009), 179.
20) Y. Funakawa, K. Seto and H. Nakamichi: *Mater. Sci. Forum*, **638-642** (2010), 3218.
21) H. W. Yen, P. Y. Chen, C. Y. Huang and J. R. Yang: *Acta Mater.*, **59** (2011), 6264.
22) Y. Daitoh, S. Torizuka and T. Hanamura: *Tetsu-to-Hagané*, **97** (2011), 480.
23) G. Miyamoto, R. Hori, B. Poorganji and T. Furuhara: *ISIJ Int.*, **51** (2011), 1733.
24) R. K. Ham: *Philos. Mag.*, **6** (1961), 1183.
25) K. Yamada, K. Sato and H. Nakamichi: *JFE Giho*, No. 13, (2006), 18.
26) H. W. Yen, C. Y. Huang and J. R. Yang: *Scr. Mater.*, **61** (2009), 616.
27) R. G. Baker and J. Nutting: *ISI Special Rep.*, No. 64 (1959), 1.
28) R. Hori: Master Thesis, Tohoku University, (2009).
29) I. B. Timokhina, P. D. Hodgson, S. P. Ringer, R. K. Zheng and E. V. Pereloma: *Scr. Mater.*, **56** (2007), 601.
30) H. Yasuhara, K. Sato, Y. Toji, M. Ohnuma, J. Suzuki and Y. Tomota: *Tetsu-to-Hagané*, **96** (2010), 545.
31) J. E. Bailey and P. B. Hirsch: *Philos. Mag.*, **5** (1960), 485.
32) N. Hansen and X. Huang: *Acta Mater.*, **46** (1998), 1827.
33) G. W. C. Kaye and T. H. Laby: Tables of Physical and Chemical Constants, 14th ed., Longman, London, (1973), 31.
34) G. Y. Chin and W. L. Mammel: *Trans. Metall. Soc. AIME*, **239** (1967), 1400.
35) E. O. Hall: *Proc. Phys. Soc.*, **B64** (1951), 747.
36) N. J. Petch: *J. Iron Steel Inst.*, **174** (1953), 25.
37) E. Orowan: Dislocations in Metals, ed. by M. Cohen, New York, AIME, (1954), 69.
38) M. F. Ashby: Physics of Strength and Plasticity, ed. by A. S. Argon, MIT Press, Massachusetts, (1969), 113.
39) T. Gradman: The Physical Metallurgy of Microalloyed Steels, Maney Publishing, London, (2002), 47.
40) T. Gladman: *Mater. Sci. Technol.*, **15** (1999), 30.
41) Y. Kobayashi, J. Takahashi and K. Kawakami: *Scr. Mater.*, **67** (2012), 854.
42) G. E. Dieter: Mechanical Metallurgy, SI Metric Ed., McGraw-Hill Book Company, London, (1988), 289.
43) M. Ashby: *Philos. Mag.*, **14** (1966), 1157.
44) M. Ashby: *Philos. Mag.*, **21** (1970), 399.
45) A. Ohmori, S. Torizuka and K. Nagai: *ISIJ Int.*, **44** (2004), 1063.
46) M. Murakami, T. Kitaura, N. Nakada, T. Toshihiro and S. Takaki: *Tetsu-to-Hagané*, **97** (2011), 152.
47) K. Yamada, H. Nakamichi, K. Sato, K. Yasunaga, T. Daio and S. Matsumura: *Tetsu-to-Hagané*, **98** (2012), 469.